PROCEEDINGS OF THE ROYAL SOCIETY A

Proc. R. Soc. A (2007) **463**, 1713–1728
doi:10.1098/rspa.2007.1844
Published online 24 April 2007

Towards an artificial olfactory mucosa for improved odour classification

By Julian W. Gardner[1,*], James A. Covington[1], Su-Lim Tan[1] and Timothy C. Pearce[2]

[1]*School of Engineering, University of Warwick, Coventry CV4 7AL, UK*
[2]*Department of Engineering, University of Leicester, Leicester LE1 7RH, UK*

Here, we report on a biologically inspired analytical system that represents a new concept in the field of machine olfaction. Specifically, this paper describes the design and fabrication of a novel sensor system, based upon the principle of 'nasal chromatography', which emulates the human olfactory mucosa. Our approach exploits the physical positioning of a series of broadly tuned sensors (equivalent to the olfactory epithelium) along the length of a planar chromatographic channel (analogous to the thin mucus coating of the nasal cavity) from which we extract both spatial (response magnitude) and temporal (retentive delay) sensor signals. Our study demonstrates that this artificial mucosa is capable of generating both spatial and temporal signals which, when combined, create a novel spatio-temporal representation of an odour. We believe that such a system not only offers improved odour discrimination over a sensor array-based electronic nose, but also shorter analysis times than conventional gas chromatographic techniques.

Keywords: electronic nose; artificial olfaction; chemical sensors; olfactory mucosa

1. Introduction

It is not uncommon for an increase in the understanding of a biological system to lead to a significant technological advance. In the evolution of the science of machine olfaction, and 'electronic nose' (e-nose) technology, there have been milestones in the areas of sensor design, sensing materials and packaging (Gardner & Bartlett 1999). These past developments have led to the commercialization of e-nose instruments and their subsequent application in a broad range of industries, including food, environmental and healthcare (Pearce *et al.* 2003). Traditional e-noses operate by making use of a small number of chemical sensors with partially overlapping sensitivities. Each sensor is tuned to a different chemical group so that when an array of sensors is presented with a complex odour its chemical components produce a response vector or odour fingerprint. Although many instruments are commercially available today, their ability to identify complex odours in real world situations is still somewhat limited. This shortcoming is further highlighted when such instruments are

* Author for correspondence (j.w.gardner@warwick.ac.uk).

Received 24 November 2006
Accepted 13 March 2007

compared to their biological counterpart, which is not only able to identify odours at lower (by orders of magnitude) concentrations but also within a background of other time-varying interfering odours.

Greater system complexity and redundancy in the biological system over and above existing technological implementations are responsible, at least in part, for its superior operating performance. The human olfactory system, for instance, has some 100 million olfactory receptors (ORs) with approximately 350 different types of receptor proteins expressed by the human genome in the olfactory epithelium (Malnic *et al.* 1999; Goldstein 2001). In contrast, an e-nose has a small number (typically less than 32) of chemical sensors in a basic chamber and a chemometric data processing algorithm. Until now researchers have concentrated predominantly on deploying different sensing materials and their chemo-reception mechanisms to approach the impressive diversity and sensitivity of ORs; however, few have researched either the physiology of the biological system to study whether it offers any advantage or studied carefully how odours should be optimally delivered to an olfactory sensing device. Here, we propose to mimic the basic structure of the input stage of the human olfactory system, specifically, emulating the properties of the olfactory mucosa.

The olfactory mucosa lies at the top of the human nasal cavity (within the superior turbinate) and comprises the olfactory epithelium and mucus layer—figure 1(*a*). This olfactory epithelium contains the receptor cells and hair-like cilia structures with the different olfactory binding proteins, which are distributed along and beneath the thin mucus layer. Various studies have demonstrated the mucus layer coating the nasal epithelium has partitioning (or gas chromatographic; GC) type properties that contributes to the coding of olfactory information (Mozell *et al.* 1987; Kent *et al.* 2003). Receptor cells distributed beneath this 'nasal chromatograph' have been shown to generate *both* spatial[1] (response magnitude) and temporal (time-delayed) signals (Kent *et al.* 1996), which are thought to give rise to the generation of a spatio-temporal map of the odourant being generated and conveyed to the olfactory bulb. It has been suggested that these signals could, plausibly, be an important factor in enhancing our ability to discriminate between similar odours (Quenet *et al.* 2001; Lysetskiy *et al.* 2002).

Such a segregated approach to odour delivery has yet to be exploited technologically but potentially offers performance gains from the spatio-temporal dynamics of the sensor population response; thereby contributing information about the stimulus. We believe that this approach will lead to significant improvement in the capability of a new generation of e-noses. For instance, such a system would offer faster analysis times over conventional GC-based methods and be able to identify simple and complex odours better than current e-nose instruments. Moreover, segregation of odours at the front end of the olfactory pathway may be a key factor in solving complex odour discrimination tasks where the system needs to be sensitive to the relationship between individual odour components existing within a blend. The challenge here is to determine how best to exploit this approach, i.e. by combining it with modern fabrication technologies to create a new architectural platform for future e-nose implementation. In this

[1] For the sake of expediency, we decided to adopt the term 'spatial' here to describe the maximum signal in odour space and to differentiate it from the simple time-delay (temporal) signal.

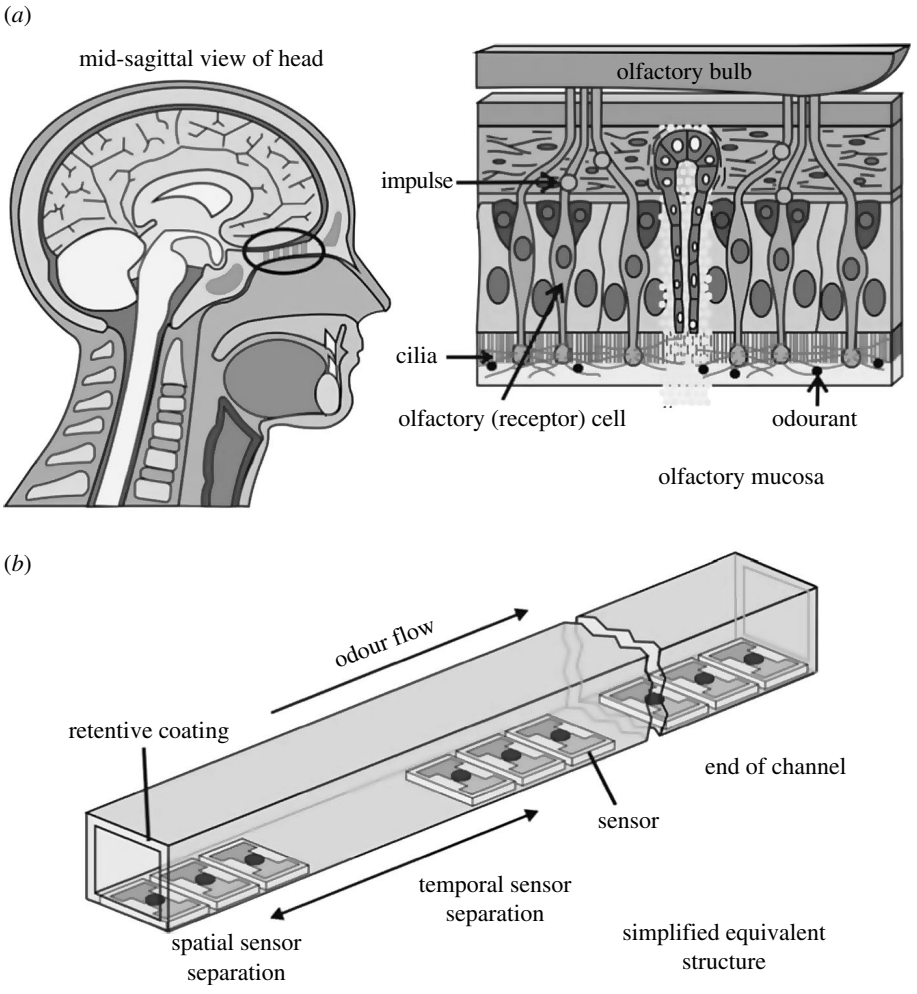

Figure 1. (*a*) Mid-sagittal view of a head showing the location of the olfactory mucosa (circled) with a detailed cross-section for part of the human olfactory mucosa showing the mucus layer and receptor cells and (*b*) our simplified equivalent structure of the artificial mucosa.

paper, we report on our initial effort to develop an artificial mucosa system, employing finite-element modelling, device fabrication and odour testing, in order to provide superior odour discrimination.

2. Artificial olfactory mucosa design and modelling

Our artificial mucosa comprises multiple chemical sensors distributed along the length of a gas chromatograph channel, as shown in figure 1*b*. GC separation relies on a layer of retentive material (stationary phase) coating the inner surface of a column or channel. When a fixed volume of compound analyte (e.g. complex odour) is injected into the column with a carrier gas, each component within the compound analyte travels along the column at a different velocity

(mobile phase), depending upon its affinity with the stationary phase. Hence, towards the end of the column, a sequence of pulses will elute representing the separated chemical components, depending on its length.

A finite-element model (FEM) was developed to investigate the characteristics of the artificial olfactory mucosa. A commercial FEM package (Femlab, Comsol, UK) was used to simulate analyte transportation and retention behaviour. A multi-physics model, employing the Navier–Stoke equation, was used to simulate laminar transport. Convection and diffusion models were used to simulate the diffusion and dispersion of the injected analyte pulse (Fontes *et al.* 2001). Diffusion was used to model the dispersion and partitioning effect of the analyte (Tan *et al.* 2006) in the coating. Partial differential equations were used for the simulations and have been described in detail elsewhere (Tan 2005). To ensure that the model was an accurate estimate of the actual phenomena, simulations of equivalent GC columns using a standard commercial GC software package were performed, hence cross-validating results with established analytical solutions. The mucosa model (1.2 m long column with 500 μm^2 cross-sectional area and 10 μm coating layer) was found to perform similarly to a GC column with errors of less than 3% in retention time and less than 9% in separation factor.

The real olfactory mucosa is relatively short (approx. 10 cm) when compared with traditional GC column lengths (approx. 10 m). Moreover, the biological system has analysis times that are drastically quicker (much less than 10 s) than both GC systems (approx. 10 min) and traditional e-nose instruments (approx. 1 min). Hence, we have chosen a reduced channel length to be closer to the human olfactory system rather than requiring complete component separation. Thus, our analysis will be performed on information that can be extracted from this shorter channel rather than seeking perfect GC-like component separation, as is likely to be the case in biology. Our artificial mucosa comprised a 2.4 m$\times$ 0.5 mm$\times$0.5 mm long rectangular channel with 40 discrete sensors of five different tunings (i.e. five different sensing materials with differing specificities). A 10 μm thick layer of Parylene C (polymonochloroparaxylylene C) was used as the retentive coating. The use of this material as a stationary phase was first introduced by Noh *et al.* (2002) and it has been shown that this material behaves as a stationary phase coating. The 40 sensors were placed into eight groups of five with each group containing the five different tunings. Details of sensor types and their placement along the channel are given in table 1. Simple polar and non-polar odours, namely ethanol and toluene, were used in the computer simulations in order to compare and optimize the operation of coated and uncoated channels.

Simulation results showed that the optimum flow velocity for column efficiency was approximately 7 cm s^{-1} for a 5 s pulse of ethanol and toluene vapour in air, although the effect of increasing flow velocity was found to be marginal on column efficiency. This velocity gave the best compromise between reducing the unwanted pulse broadening in which the faster the flow is the less the odour pulse front has time to diffuse out while traversing down the channel, and increasing the desired retention effect. In the latter mechanism, the lower the flow velocity is, the better is the separation of chemical components for a complex odour. These simulations give the analyte concentration profiles at the different physical locations rather than the corresponding sensor responses.

Table 1. Sensor placements within the artificial olfactory mucosa for both the simulations and fabricated system. PEVA, polyethylene-co-vinyl acetate; PSB, polystyrene-co-butadiene; PEG, polyethyleneglycol; PCL, polycaprolactone; PVPH, poly 4-vinyl phenol.

no.	distance (mm)	type	no.	distance (mm)	type
S1	10	PEVA	S21	1260	PEVA
S2	30	PSB	S22	1280	PSB
S3	50	PEG	S23	1300	PEG
S4	70	PCL	S24	1320	PCL
S5	90	PVPH	S25	1340	PVPH
S6	240	PEVA	S26	1620	PEVA
S7	260	PSB	S27	1640	PSB
S8	280	PEG	S28	1660	PEG
S9	300	PCL	S29	1680	PCL
S10	320	PVPH	S30	1700	PVPH
S11	570	PEVA	S31	1950	PEVA
S12	590	PSB	S32	1970	PSB
S13	610	PEG	S33	1990	PEG
S14	630	PCL	S34	2010	PCL
S15	650	PVPH	S35	2030	PVPH
S16	930	PEVA	S36	2180	PEVA
S17	950	PSB	S37	2200	PSB
S18	970	PEG	S38	2220	PEG
S19	990	PCL	S39	2240	PCL
S20	1010	PVPH	S40	2260	PVPH

In order to obtain the complete system model, the sensor responses were coupled to the analyte profiles. For simplicity, an analytical method (defined by equations (2.1) and (2.2)) was used to model the dynamic response characteristics of previously tested chemical sensors. Both the finite-element simulations and the fabricated system used polymer composite sensing materials, in a resistive configuration, as the odour-sensitive layer. These composites comprise electrically conducting carbon nanospheres within a non-conducting polymer binder. Thus, the carbon endows measurable electrical conductivity to the resultant composite material. These sensing materials are believed to operate through a chemo-mechanical effect, where the reversible absorption of an analyte results in a physical swelling of the polymer. The swelling reduces the mobility of electrons hopping between nanospheres within the bulk material and thus increases the electrical resistance of the film. These sensing materials were chosen owing to their rapid (approx. 100 ms) response time, ease of deposition, room temperature operation and the wide variety of available polymers. The response magnitude and response time, to pulses of ethanol and toluene vapour in air, were measured by the five polymer/carbon black composite sensors (mixed 80 : 20 by weight polystyrene-co-butadiene (PSB), polyethylene-co-vinyl acetate (PEVA), polyethyleneglycol (PEG), polycaprolactone (PCL) and poly 4-vinyl phenol (PVPH)). Experiments were carried out at different flow velocities (up to 1600 cm s^{-1}), at a temperature of 30 ± 2°C, and relative humidity of 40 ± 5%, while the responses (defined as the change in resistance from the baseline value in air) were measured.

Table 2. Values of model 'on' parameters estimated by fitting experimental data from PSB, PEVA, PEG, PCL and PVPH composite sensor responses to pulses of ethanol and toluene vapour in air. R is the Pearson correlation coefficient with a perfect fit giving a value of one. Fitted values for the 'off' parameters are not employed in the data analysis performed here but may be found in Tan (2005).

	ethanol			toluene		
sensor type	R_{ON}	τ_{ON}	R^2	R_{ON}	τ_{ON}	R^2
PSB	0.5346	0.3568	0.8638	3.3282	0.4062	0.9902
PEVA	2.6793	0.7229	0.9626	20.9653	0.5349	0.9870
PEG	35.1677	0.0630	0.9945	32.5009	0.1445	0.9948
PCL	0.8580	0.103	0.9477	7.7427	0.0807	0.9964
PVPH	2.1748	0.1887	0.9928	2.1630	0.1881	0.9950

These were carried out in a purpose-designed micro-chamber system to help create suitable boundary conditions for simple laminar plug flow. Details of the characterization and test systems are described in Tan (2005). A number of studies have suggested that the response of these sensors can be approximated to a bilinear exponential model (Gardner *et al.* 1995, 1999). Using this simple model, the response of a sensor to a step increase in odour concentration c or 'on transient' is given by

$$R(c,t) = R_{ON}(c)[1 - e^{-\tau_{ON}t}], \tag{2.1}$$

where R_{ON} is the maximum response magnitude (i.e. at odour concentration c_o) and τ_{ON} is the characteristic rise time. Conversely, the 'off transient' is given by

$$R(c,t) = R_{OFF}(c)e^{-\tau_{OFF}t}, \tag{2.2}$$

where R_{OFF} is the decay magnitude and τ_{OFF} is the characteristic decay time. In practice, R_{ON} and R_{OFF} have very similar magnitudes, whereas τ_{OFF} is usually much larger than τ_{ON}. Table 2 gives the values of the different 'on' parameters estimated by fitting the model to experimental data. Figure 2 shows the sensor response magnitude and profile (generated from these fitted model parameters) for the five types of sensor responding to a rectangular pulse of (i) ethanol vapour and (ii) toluene vapour in air. The odour pulse introduced to the channel had a flow velocity of 50 cm s^{-1}, a pulse width of 5 s, vapour concentration of 0.05 mol m^{-3} and was at a temperature of 25°C. In general, the sensors' responses are computed from the analyte concentration profile and bilinear sensor model at various locations as the pulse traverses down the channel. (N.B. most commercial e-nose instruments only use the 'spatial' data shown in figure 2 for odour discrimination; in other words, the different magnitudes of sensor response at some moment in time).

Figure 3(a) shows the theoretical concentration profiles at five different points, where sensors (e.g. S11) are located along the channel, when a 5 s ethanol vapour pulse is injected into the artificial olfactory mucosa (test conditions as before, stationary phase thickness is 10 μm). As stated above, the temporal delay is caused by the analyte partitioning into the stationary phase coating by differing amounts. The actual time at which analytes reach a sensor is in general odour

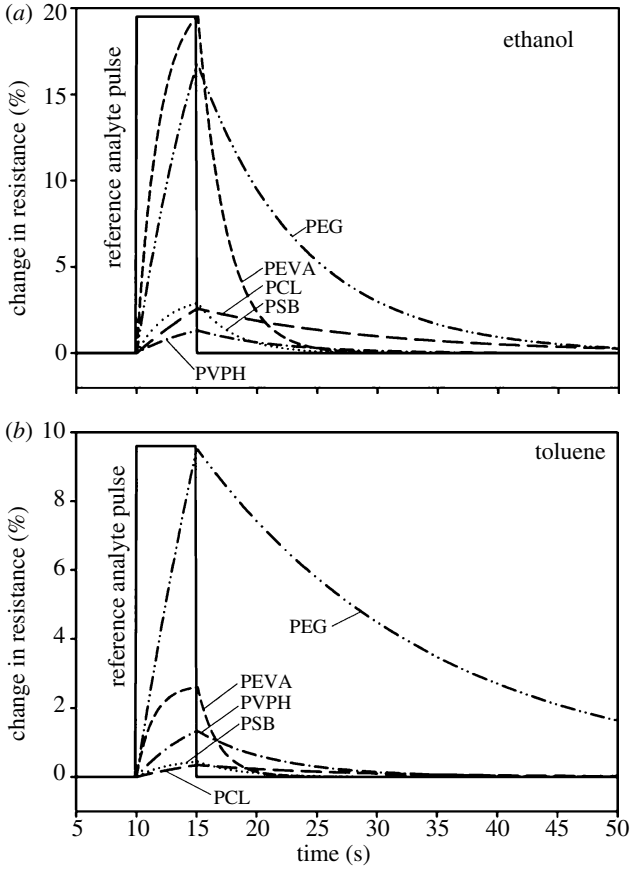

Figure 2. Simulated responses of PSB-, PEVA-, PEG-, PCL- and PVPH-based resistive sensors. Sensor response (as percentage change in resistance) to 5 s pulse of (*a*) ethanol vapour and (*b*) toluene vapour in air against time (s).

dependent and more specifically related to the polarity of the odour molecule. The responses of the sensors located at these points along the channel are shown in figure 3*b*. The temporal delay from sensor S2 to S39 (measured from when the signal drops to 50% of its response magnitude) was found to be 38.7 s for ethanol and 340.9 s for toluene vapour.

The results of these simulations show that an artificial mucosa, based on these channel dimensions and stationary phase coating, should be able to produce spatial–temporal profiles suitable for simple linear odour discrimination.

3. Artificial olfactory mucosa fabrication

Our fabricated artificial olfactory mucosa consisted of 40 discrete polymer/carbon black composite chemoresistive sensors (details are given in table 1), a printed circuit board (PCB) base, into which the sensors were mounted and connected, and two different lids (with and without stationary phase coating, fabricated from polyester, RS Components Ltd). The lids' dimensions were

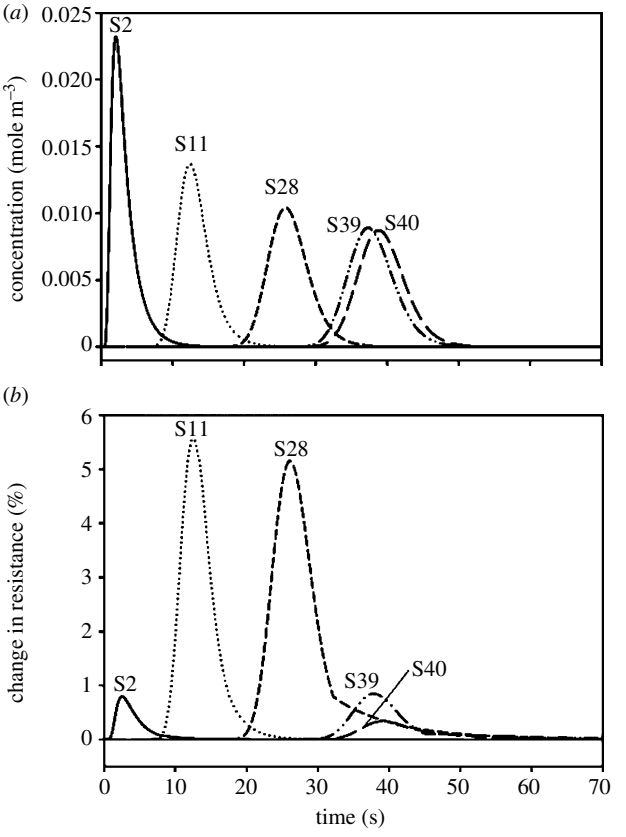

Figure 3. Artificial olfactory mucosa sensor responses to ethanol vapour. (*a*) Ethanol vapour profiles of five identical sensors located at five different positions along the GC microchannel. (*b*) Five different polymer types of sensors responding to ethanol vapour at these locations. The signal for sensor S2 is much lower than the others because the polymer (PSB) responds much more to toluene than ethanol.

10×200×235 mm with a machined channel (channel of dimensions 2.4 m× 0.5 mm×0.5 mm) laid out in a serpentine pattern[2]. The sensors were fabricated using custom 3″ wafer silicon processing technology within the School of Engineering, University of Warwick. Each device was 2.5×4.0 mm in size and consisted of a pair of thin coplanar gold electrodes on a SiO_2/Si substrate with an electrode length of 1.0 mm and an inter-electrode gap of 75 μm.

In our final experimental set-up, 10 different polymers were used, in comparison with the five employed in the computer simulations, in order to enhance even further the system's ability to discriminate between different odours. The 10 recipes for these polymers or 'tunings' are given in table 3. The polymer materials were supplied by Sigma Aldrich (UK) and the carbon black (Black Pearls 2000) material was supplied by Cabot Corporation (USA). The polymers were either in powder form or small crystals while the carbon black contained nanospheres with diameters varying from 50 to 80 nm. The polymers

[2] An exact layout of the channel pattern may be found in Tan (2005).

Table 3. Polymer-composite sensing material recipes for 10 different sensor types.

no.	polymer	polymer mass (g)	mass of carbon black (g)	solvent (20 ml)
1	poly styrene-co-butadiene (PSB)	0.7	0.175	toluene
2	poly ethylene-co-vinyl acetate (PEVA)	1.2	0.300	toluene
3	poly ethylene glycol (PEG)	1.2	0.300	ethanol
4	poly caprolactone (PCL)	1.2	0.300	toluene
5	poly 4-vinyl phenol (PVPH)	1.2	0.300	ethanol
6	poly 9-vinylcarbazole (PVC)	0.3	0.300	toluene
7	poly vinyl pyrrolidone (PVPD)	0.3	0.300	ethanol
8	poly(bisphenol-A-carbonate) (PBA)	0.7	0.175	dichloromethane
9	poly(sulphane) (PSF)	0.7	0.175	dichloromethane
10	poly(chloro-*p*-xylylene) (PCX)	1.2	0.300	toluene

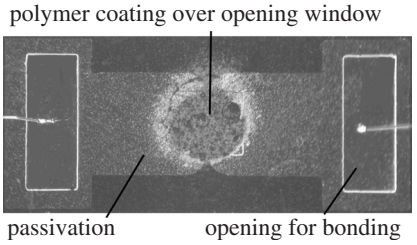

Figure 4. Photograph of actual odour sensor showing the polymer coating above a pair of electrodes.

were first dissolved in their respective solvent overnight with the aid of a magnetic stirrer (SEA, UK) at an elevated temperature of 50°C. Carbon black was then added and the mixture sonicated for 10 min using a flask shaker (Griffin and George, UK). The mixture was then deposited onto the sensors using an airbrush (HP-BC Iwata, Japan) controlled with a micro-spraying system (RS precision liquid dispenser, UK). The deposition area was defined by a mechanical mask, with a circular hole of 1.0 mm diameter, aligned by a purpose-built X–Y stage. The airbrush was held approximately 10–15 cm away from the mask and several passes were made depending on the desired thickness (or resistance). This actually resulted in a circular coating of typically 1.5 mm in diameter. The electrical resistances of the composite polymer sensors were controlled through the deposition process to a value of approximately 5 kΩ with a typical film thickness of approximately 20 μm ($\pm 25\%$). Finally, figure 4 shows a photograph of an odour sensor with the composite polymer coating clearly visible.

After the sensors' fabrication, the devices were mounted into slots machined into the PCB base and gold wire bonded to copper tracks etched into the top. The sensor placements were identical to those given in table 1, though now the sensors S6–S10, S16–S20, S26–S30 and S36–S40 were replaced with poly(9-vinylcarbazole) (PVC), poly(vinyl phenol) (PVPD), poly(bisphenol-A-carbonate) (PBA), poly(sulphane) (PSF) and poly(chloro-*p*-xylylene) (PCX), with each block of five sensors replaced in this order. The resistance of the sensors was measured with a custom-built electronic circuit in which the sensor was the

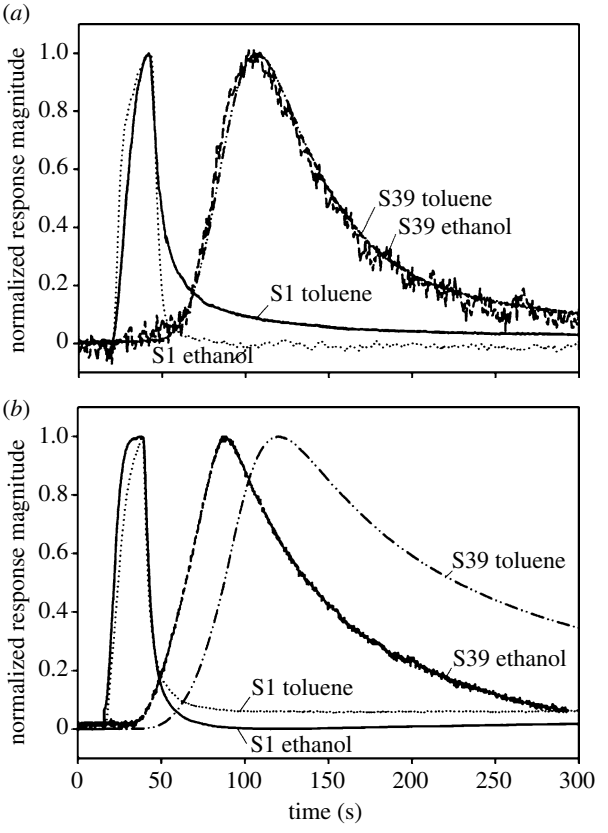

Figure 5. Observed responses of sensor S1 (front of column) and S39 (end of column) for an (*a*) uncoated and (*b*) coated channel to pulses of both toluene and ethanol vapour in air. From S39, it is evident that the coated column separates out the vapour components in retention time.

feedback resistor of an operational amplifier circuit in an inverting configuration. The reference input resistor is connected to a -2.5 V reference voltage source in order to produce a positive output to a 16 bit analogue-to-digital converter (ADC). The retentive layer used to coat the channel, as used in the simulations, was parylene C. This was deposited using a commercial evaporation technique (PDS 2010 Labcoater 2, Specialty Coating Systems, Indianapolis, USA). The machine performs deposition under a vacuum at room temperature, taking approximately 3.5 h to deposit a 10 μm thick film.

4. Experimental results and discussion

The final design of the artificial olfactory mucosa was first tested with both uncoated and coated lids to demonstrate that the retentive coating selectively delayed vapours along the channel. Simple polar and non-polar odours (ethanol and toluene vapour in air, 10 s pulse, test temperature 22 ± 2°C, humidity of 40 ± 5% relative humidity (RH)) were used to validate the operation of the channel and to make a direct comparison with the simulations. The results of

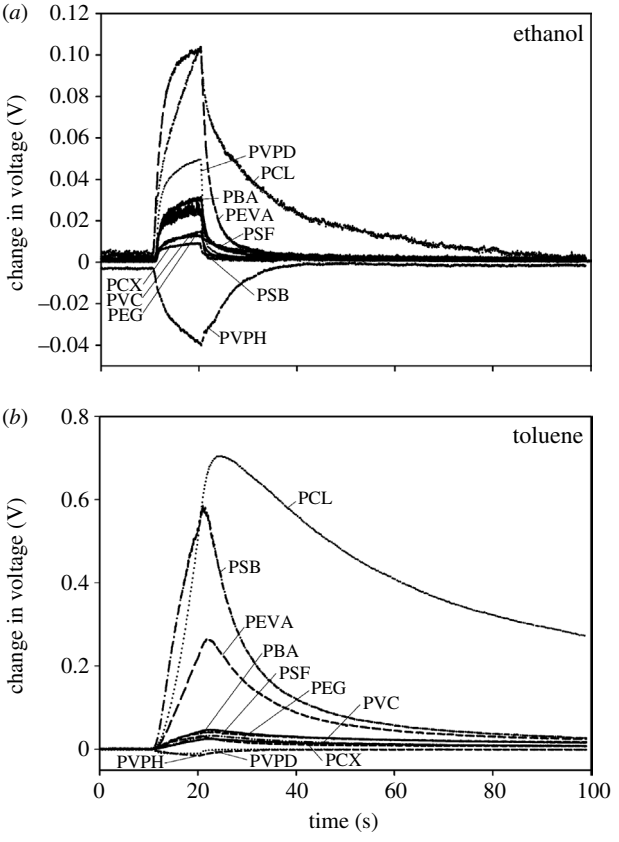

Figure 6. Observed response of different types of sensors responding to simple analytes, i.e. spatial signals. Sensor responses to 10 s pulse of (*a*) ethanol vapour and (*b*) toluene vapour in air.

these tests are shown in figure 5, where the responses of the sensors at the front (sensor S1) and rear (sensor S39) of the channel are shown for both uncoated (figure 5*a*) and coated (figure 5*b*) lids. Comparing the uncoated and coated lid sensor responses for sensor S1, it was observed as expected that both the ethanol and the toluene vapour pulses reached the sensor simultaneously. While for sensor S39, at the end of the channel, for the uncoated lid the ethanol and toluene pulses reached the sensor simultaneously (peaks at $t \sim 120$ s), though for the coated channel a 31 s delay was observed between the two analytes. These results agree well with the finite-element simulation results given above. The data used in figure 5 have been normalized to emphasize the temporal time delay, hence the spatial height information is not seen.

In order to evaluate further the artificial mucosa, additional experiments were performed to ensure that the system was capable of producing significant diversity in both spatial and temporal signals. These experiments used both light simple odours (ethanol and toluene vapour) and heavier/complex odours (essential oils, i.e. peppermint and vanilla, also milk, cream, banana and 50 : 50 mixture by volume of peppermint/vanilla and cream/milk). Figure 6*a*,*b* shows the response of the first 10 odour sensors to a 10 s pulse of ethanol and toluene vapour in air, respectively. The response profiles and magnitude

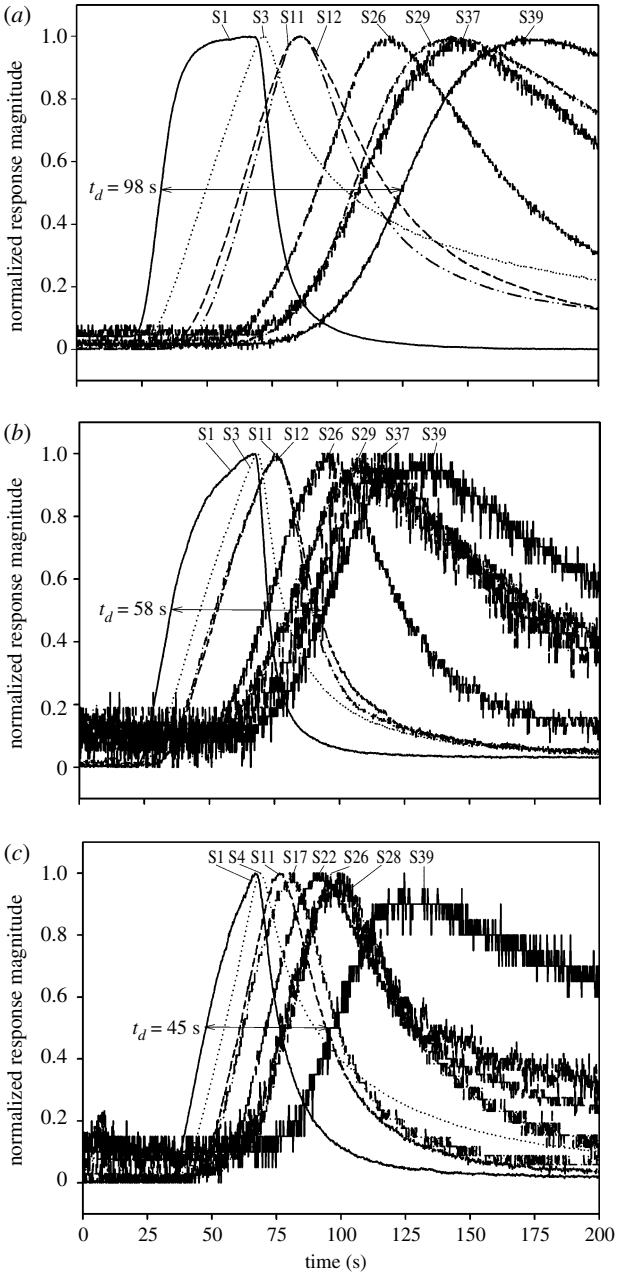

Figure 7. Observed temporal signals of sensors responding to simple and complex analytes. (*a*) Normalized sensor responses to toluene vapour in air. (*b*) Normalized sensor responses to ethanol vapour in air. (*c*) Normalized sensor response to peppermint essence vapour in air.

information correspond to the spatial information given by our system. Clearly, there is considerable diversity in the response. These experiments were conducted at a flow rate of 25 ml min^{-1} and a pulse width of 25 s with five repetitions at room temperature (25 ± 2°C, 40 ± 5% RH).

Table 4. Spatial and temporal sensor response values for both simple and complex odours. (The spatial response magnitude R_{ON} is defined here as the change in sensor output voltage; and the temporal response as time taken for the odour pulse to travel along the channel.)

sensor number	toluene	ethanol	toluene/ ethanol	peppermint	vanilla	peppermint/ vanilla	banana	milk
spatial (V)								
S1	2.814	0.454	1.681	1.114	0.282	0.674	0.140	0.166
S12	1.169	0.218	0.610	0.635	0.102	0.347	0.049	0.052
S19	2.220	0.399	1.098	1.030	1.141	0.547	0.061	0.064
S28	0.360	0.276	0.266	0.556	0.085	0.292	0.108	0.143
S40	0.135	0.103	0.095	0.335	0.133	0.236	0.143	0.158
temporal (s)								
S1	12.42	12.66	12.89	6.48	7.41	8.96	8.70	5.43
S12	23.36	16.37	22.45	13.35	12.47	14.92	13.60	13.75
S19	26.22	17.61	24.61	14.95	14.18	15.64	15.94	16.62
S28	33.64	20.53	26.25	16.08	13.41	16.61	25.74	30.41
S40	36.15	21.52	27.19	17.45	13.73	17.82	23.35	24.61

Figure 7 shows the normalized response of three sets of sensor responses to pulses of (i) toluene vapour, (ii) ethanol vapour and (iii) peppermint essence vapour, showing temporal information from the system. Eight different sensor responses along the channel are depicted to illustrate different spatial signals (S1 and S39 provide the two extremes). Clearly, the sensors have responded in sequence according to their placements. As stated above, the time at which the sensor response magnitude reaches 50% is used for comparing the retention time delay (temporal delay). The relative retention time between S1 and S39 is approximately 92 s for toluene vapour, 58 s for ethanol vapour and 45 s for peppermint essence vapour. Using this temporal information, different analytes can be identified. Comparing these results with those obtained by the finite-element simulation, the general trend is similar. Table 4 gives the spatial and the temporal delay signals from a set of sensors (S2, S12, S19, S28 and S39) along the column for both the simple and the complex odours. These variables were used in a principal components analysis (PCA) to determine linear separability in multivariate space. Analyses were performed using the spatial data alone, the temporal data alone and the combined spatio-temporal data. Figure 8*a* shows a plot of the first two principal components of the spatial data only. In this case, linear classification is reasonable for all of the analytes except milk and banana. Figure 8*b* shows a PCA plot of only the temporal data and overall the clusters are less tight. However, when the milk and banana samples do now give separate clusters classes although the variation within each cluster is much larger than that from other test analytes. Finally, figure 8*c* shows the results when both the spatial and the temporal data of the sensors are included in the PCA. It is evident that the general performance is better than the temporal data and closer to that of spatial data. On closer inspection, the clusters for banana and milk samples are now not only separable in multivariate space but also much smaller

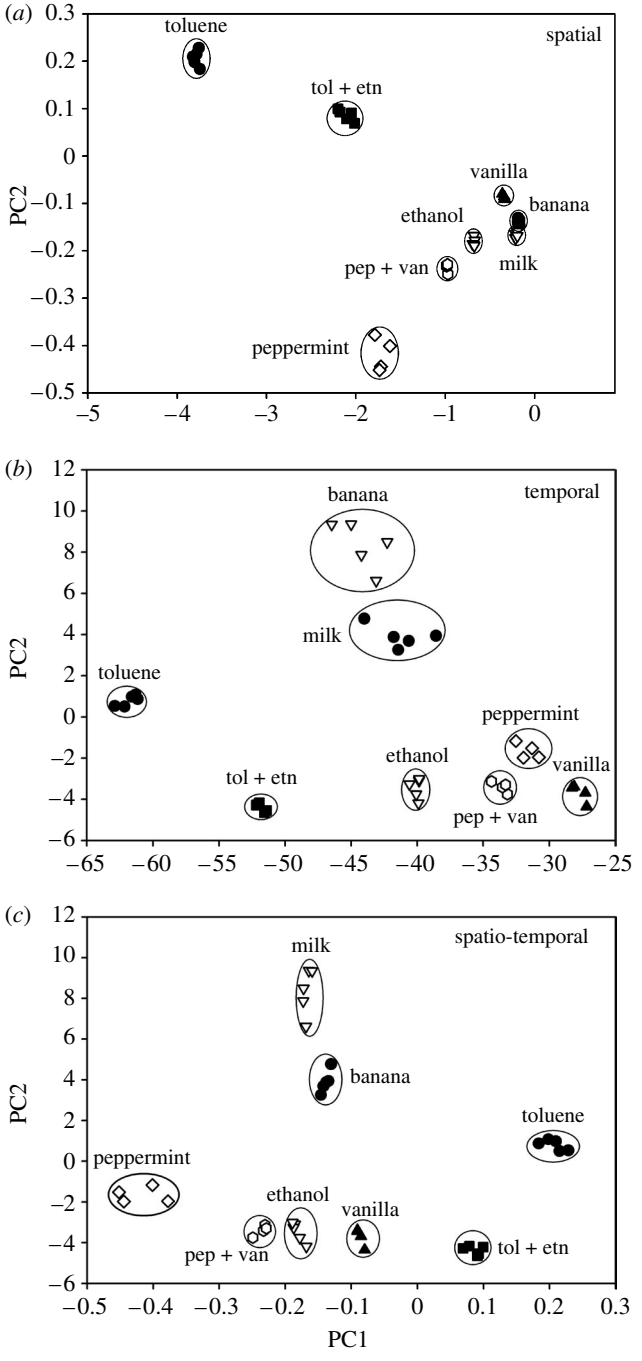

Figure 8. PCA plots of data recorded from five different odour sensors in the artificial olfactory mucosa. (*a*) Spatial (response magnitude, ΔV) data only. (*b*) Temporal (time at 50% of ΔV) data only. (*c*) Combined spatio-temporal data for five odour sensors.

in width thus providing a better ratio of cluster separation to cluster width (unlike for the spatial data). In analysis of variance with repeated measures (ANOVAR), this is Snecodor's *F*-test and is important in defining the statistical confidence level for classifying two clusters as belonging to different classes. Therefore, the results show that the spatio-temporal data, which emulate the nasal chromatography principle exhibited in biological olfactory system, provide better discrimination than either spatial or temporal signals alone. Further and more advanced data analysis techniques have been developed and also show improved performance of the spatio-temporal data and these will be published in a subsequent article.

5. Conclusions

A novel artificial olfactory mucosa has been designed, simulated and fabricated to mimic the nasal chromatography phenomenon that has been observed in the mammalian olfactory system. Our system aims to replicate the biological process where spatio-temporal signals are extracted by receptor cells placed below the mucus layer within the nasal cavity. Using this concept, a system combining 40 polymer-composite sensors of 10 different tunings were placed along a 2.4 m long polymer-coated channel. The distributed sensor system was tested with both simple and complex odours in order to examine its capability to generate both spatial and temporal signals. The results showed that the 'e-mucosa' system can produce such types of signals for different odours, with temporal delays of up to 92 s. Multivariate analysis also verified that spatial and temporal signals could be used individually for odour discrimination, but that the combined spatio-temporal signals gave an even better performance. Current e-nose technology generally uses spatial signals and the use of spatial/temporal signals based on an artificial olfactory mucosa has clearly been demonstrated to be superior. Future work will be directed towards the analysis of more challenging odour discrimination problems (e.g. odour segmentation) and this will require the development of more advanced topologies and nonlinear spatio-temporal signal processing techniques.

The authors would like to thank the Engineering and Physical Research Council (UK) for financial support of this research project (grant no. GR/R37975/01).

References

Fontes, E., Byrne, P., Sundqvist, J., Bosander, P. & Marklund, M. 2001 *Femlab chemical engineering user manual (version 2.1)*. Palo Alto, CA: Comsol.

Gardner, J. W. & Bartlett, P. N. 1999 *Electronic noses: principles and applications*, pp. 1–245. Oxford, UK: Oxford University Press.

Gardner, J. W., Bartlett, P. N. & Pratt, K. F. E. 1995 Modelling of gas-sensitive conducting polymer devices. *IEE Proc.-Circ. Dev. Syst.* **142**, 321–333. (doi:10.1049/ip-cds:19952170)

Gardner, J. W., Hines, E. L., Molinier, F., Bartlett, P. N. & Mottram, T. T. 1999 Prediction of health of dairy cattle from breath samples using neural network with parametric model of dynamic response of array of semiconducting gas sensors. *Proc. IEE Sci. Meas. Technol.* **146**, 102–106. (doi:10.1049/ip-smt:19990100)

Goldstein, B. 2001 *Sensation and perception*, p. 704. 6th edn. Belmont, CA: Wadsworth Publishing Company.

Kent, P. F., Mozell, M. M., Murphy, S. J. & Hornung, D. E. 1996 The interaction of imposed and inherent olfactory mucosal activity patterns and their composite representation in a mammalian species using voltage-sensitive dyes. *J. Neurosci.* **16**, 345–353.

Kent, P. F., Mozell, M. M., Youngentob, S. L. & Yurco, P. 2003 Mucosal activity patterns as a basis for olfactory discrimination: comparing behavior and optical recordings. *Brain Res.* **981**, 1–11. (doi:10.1016/S0006-8993(03)02512-5)

Lysetskiy, M., Lozowski, A. & Zurada, J. M. 2002 Invariant recognition of spatio-temporal patterns in the olfactory system model. *Neural Process. Lett.* **15**, 225–234. (doi:10.1023/A:1015773115997)

Malnic, B., Hirono, J., Sato, T. & Buck, L. B. 1999 Combinatorial receptor codes for odors. *Cell* **96**, 713–723. (doi:10.1016/S0092-8674(00)80581-4)

Mozell, M. M., Sheehe, P. R., Hornung, D. E., Kent, P. F., Youngentob, S. L. & Murphy, S. J. 1987 Imposed and inherent mucosal activity patterns. Their composite representation of olfactory stimuli. *J. Gen. Physiol.* **90**, 625–650. (doi:10.1085/jgp.90.5.625)

Noh, H. S., Hesketh, P. J. & Frye-Mason, G. C. 2002 Parylene C gas chromatographic column for rapid thermal cycling. *J. Microelectromech. Syst.* **11**, 718–725. (doi:10.1109/JMEMS.2002.805052)

Pearce, T. C., Schiffman, S. S., Nagle, H. T. & Gardner, J. W. 2003 *Handbook of machine olfaction*, pp. 419–577. Dordrecht, The Netherlands: Wiley-VCH.

Quenet, E. B., Horn, D. & Dreyfus, G. 2001 Temporal coding in an olfactory oscillatory model. *Neurocomputing* **38–40**, 831–836. (doi:10.1016/S0925-2312(01)00469-6)

Tan, S. L. 2005 Smart chemical sensing microsystem: towards a nose-on-a-chip. PhD thesis, University of Warwick, Coventry, UK.

Tan, S. L., Covington, J. A. & Gardner, J. W. 2006 Velocity-optimised diffusion for ultra-fast polymer-based resistive gas sensors. *IEE Proc. Sci. Meas. Technol.* **153**, 64–100. (doi:10.1049/ip-smt:20050077)